2012
International Symposium on Power Electronics,
Electrical Drives, Automation and Motion

An Ultrafast EV Charging Station Demonstrator

H. Hõimoja*, A. Rufer*, G. Dziechciaruk**, and A. Vezzini**
*Laboratoire d'électronique industrielle, EPFL-STI-LEI, Station 11, 1015 Lausanne (*Switzerland*)
**Labor der Industrieelektronik, BFH-TI-LIE, Quellgasse 21, 2501 Biel (*Switzerland*)

***Abstract* — This paper deals with the design of a grid-friendly ultrafast electric vehicle charging demonstrator. High charging power and short charging times impose peaks to an electricity distribution system, which necessitate over-dimensioning of the grid connection. A mitigation option lies in partial decoupling the load from the grid, achieved with the application of energy storage elements. A calculation methodology for energy storage elements is proposed and their interconnection possibilities to an ultrafast EV charging spot discussed.**

***Index Terms* — electric vehicles, energy storage, ultrafast charging.**

I. INTRODUCTION

An inherent obstacle before a major breakthrough to the market of the electric vehicles (EV) has set itself inside the onboard traction energy storage, limiting the vehicle's autonomy and autonomy flowrate. The latter term refers in this paper to the distance gained per minute of recharging. To emphasize the situation, a comparison between a small fuel efficient family car and its electric counterpart is drawn in Table I.

TABLE I. A COMPARISON BETWEEN DIESEL AND ELECTRIC VEHICLES

Parameter	Diesel car	Electric vehicle
Consumption	5 l / 100 km	15 kW•h / 100 km
Tank capacity	45 l	24 kW•h
Autonomy	900 km	160 km
Tanking speed	35 l/min	50 kW
Autonomy flowrate	700 km/min	4 km/min

The comparison in Table I allows concluding preliminarily that one liter of diesel fuel equals around 3 kW·h of tank-to-wheel (TTW) electrical energy. Actually, the onboard battery supplies not only traction power, but also heating, cruise control, air conditioning and other auxiliaries, which result in an additional load of up to 30 % [1]. Simple calculations show, that an EV should have a battery capacity of 135 kW·h and charging power of 6.3 MW to match the autonomy and autonomy flowrate of an equivalent diesel car. With the actual and tangible energy storage technologies as well as with power system limitations, these values are not reachable.

However, reaching the autonomy values should not be a final objective, as no driver under normal conditions would cover 900 km without any intermediate stops. The recent studies on drivers' habits demonstrate, that a daily distance for 80 % of all cases does not exceed 50 km, which makes conventional slow (6 h…8 h) recharging in domestic conditions possible [2]. For those, whose trips exceed the EV autonomy, long charging times even with the available "quick" chargers resulting in prolonged travel times make the all-electric vehicles unattractive. Thus, to make more ground for the electromobility, charging times must be shortened in order to compete with the average speed of a thermally powered car. The objective charging time 5 minutes, aimed by the authors, brings along additional requirements to the hardware. Whereas a limited demonstrator is discussed here, an ampler deployment of ultrafast charging issues at higher EV market penetration has been studied based on statistical analysis [3].

This work was supported by the Competence Centre Energy and Mobility (CCEM) and Swisselectric Research

II. STATE OF THE ART

Internationally, the requirements on fast charging installations are defined by IEC 61851-23, setting the standards for dc charging from an external charger [4]. One of its implementations is the CHAdeMO method, approved by several vehicle manufacturers [5], [6]. With CHAdeMO, the charging time is externally limited by the allowable current and voltage of the connector, 125 A and 500 V, respectively. Thus, an average EV needs 20 to 30 minutes for recharging from zero to 80 % of its rated capacity. This maximum state of charge (SoC) value at high charging rates is caused by utilizing only the constant current part of the battery charging curve (Fig. 1), where the charging is interrupted at the terminal voltage cutoff level in order not to damage the battery. The remaining 20 % can be delivered at constant voltage; this process has, however, an asymptotic character.

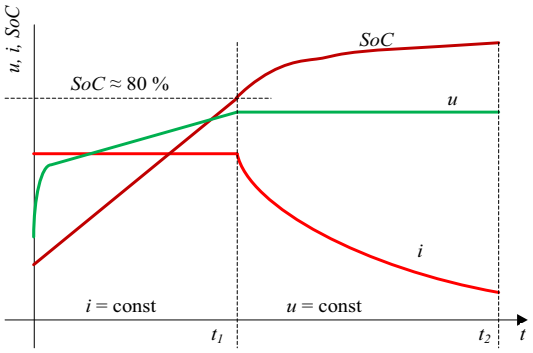

Fig. 1. A typical battery charging curve [7]

As the main objective of ultrafast charging is to remarkably shorten the recharging time t_{ch} in comparison to the actual driving time t_{dr}, their values must be expressed first.

The driving time $t_{dr,i}$ from charging spot *i-1* to charging spot *i* depends on the rated battery capacity E_{EV} expressed in kW·h, energy consumption at given speed

978-1-4673-1301-8/12/$31.00 ©2012 IEEE

E_{100} expressed in kW·h / 100 km, vehicle's road speed v expressed in km/h, initial state of charge after previous recharging $SoC_{start,i-1}$ and final state of charge before next charging $SoC_{stop,i}$:

$$t_{dr,i}(v) = E_{EV} \cdot \frac{SoC_{start,i-1} - SoC_{stop,i}}{E_{100}(v) \cdot v} \quad (1)$$

The charging time $t_{ch,i}$ in charging spot i depends on E_{EV}, $SoC_{stop,i}$, obtained state of charge $SoC_{start,i}$ and available charging power $P_{ch,i}$ (for simplification, charging power is taken constant):

$$t_{ch,i} = E_{EV} \cdot \frac{SoC_{start,i} - SoC_{stop,i}}{P_{ch,i}} \quad (2)$$

Equation (1) is rather a hint for economic driving, as the longest range is achieved by a proper selection of driving pattern, departing with the maximum available charge and continuing until the full depletion of the battery. As self-evident and expressed by (2), the charging time depends on the available charging power and battery capacity utilization.

The average speed v_{av} is defined by the road speed and times t_{dr} and t_{ch}. It can be analytically expressed, that the same average speed can be kept while charging more often and utilizing only the partial capacity of the battery:

$$v_{av,i} = v \cdot \frac{t_{dr,i}}{t_{dr,i} + t_{ch,i}} \quad (3)$$

An illustrative comparison for existing CHAdeMO method and perspective ultrafast charging option is given in Table II. For demonstration, iMiEV data are chosen [8]. Dividing the autonomy value with objective charging time yields the autonomy flowrate 17 km/min.

TABLE II. DRIVING AND CHARGING TIMES FOR IMIEV

Parameter	CHAdeMO value	5 min objective
E_{EV}	16 kW·h	
$SoC_{start,i-1}$	80 %	
$SoC_{start,i}$	80 %	
$SoC_{stop,i}$	0	
v	90 km/h	
$E_{100}(v)$	15 kW·h/100 km	
t_{dr}	57 min	
Autonomy	85 km	
t_{ch}	30 min	5 min
v_{av}	59 km/h	82 km/h

III. INFLUENCE ON THE GRID

During the objective 5 min recharging, the grid load is defined by the battery rated capacity, maximally reachable SoC at the given charging rate and related losses. In subsections below, the charging power flow will be explained in more detail.

A. Battery losses

Losses inside a battery comprise the internal resistance of the cells R_{cell} and interconnection resistances R_{con}. In a factory-assembled battery pack, the interconnection resistances can be considered negligible as compared to internal resistances: $\Sigma R_{con} << \Sigma R_{cell}$. For simplification, R_{cell} is considered to be constant and independent of the SoC and age; thus the power dissipation:

$$P_{loss,EV} = \frac{n_{cell,s}}{n_{cell,p}} \cdot R_{cell} \cdot i_{ch}^2 \quad (4)$$

In (4) $n_{cell,s}$ is the number of serial cells in the battery, $n_{cell,p}$ number of parallel strings and i_{ch} the charging current. The i_{ch}, in turn, depends on the EV battery coulomb capacity Q_{EV} expressed in A·h, objective charging time t_{ch} expressed in minutes and available reachable EV SoC range ΔSoC_{EV}:

$$i_{ch} = \frac{Q_{EV}}{t_{ch}} \cdot 60 \cdot \Delta SoC_{EV} \quad (5)$$

The manufacturers often prefer to demonstrate the relative charging and discharging currents, i.e. the current and coulomb capacity ratio instead of time:

$$i_{ch}^* = \frac{i_{ch}}{Q_{EV}} \quad (6)$$

For (6), the right dimension should be h^{-1}. Battery manufacturers, however, refer to this value as C-rate, giving e.g. the characteristics for 0.5 C, 1 C, 10 C etc. To avoid confusion with the unit for electric charge – the coulomb – this expression should not be promoted.

B. Power from the grid

The charging power from the grid P_g depends on the useful power P_u cumulating in the battery, battery losses $P_{loss,EV}$ and charging converter efficiency η_{conv}. The charger itself, depicted in Fig. 2, comprises two-stage conversion: ac/dc and isolated dc/dc for ripple reduction and power factor correction [9].

$$P_g = \frac{u_{EV} \cdot i_{ch}}{\eta_{conv}} = n_{cell,s} \cdot \frac{u_{cell} \cdot i_{ch}}{\eta_{conv}} \quad (7)$$

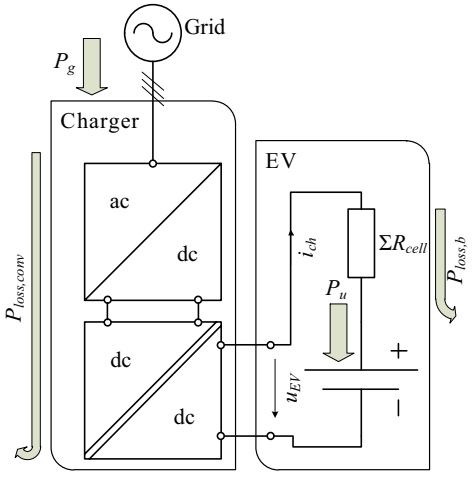

Fig. 2. A typical external EV dc charger layout

As seen from Fig. 1, the EV battery terminal voltage u_{EV} changes during charging process in a nonlinear manner, depending on the actual SoC. As i_{ch} = const, the power curve follows that of the voltage, reaching its maximum at charging termination point.

C. Calculation example

The following example in Table III is based on the data of LEV50 cells, used in small vehicles like Mitsubishi iMiEV, Peugeot iOn and Citroën C-Zero [10]. It is further assumed, that the battery with given

parameters is capable of absorbing the same energy as by CHAdeMO,during the given timeframe of 5 minutes.

TABLE III. DATA FOR IMIEV BATTERY CHARGING

Parameter	Value
$n_{cell,s}$	88
$n_{cell,p}$	1
Q_{EV}	50 A·h
E_{EV}	16 kW·h
R_{cell}	1 mΩ
ΔSoC_{EV}	80 %
t_{ch}	5 min
i_{ch}	480 A
$u_{cell,rated}$	3.7 V
$u_{cell,max}$	4.1 V
η_{conv}	95 %
$P_{loss,EV}$	20.3 kW
$P_{g,av}$	165 kW
$P_{g,max}$	183 kW

Thus, for the given example, the necessary grid connection would be 183 kW. At $\cos\varphi \approx 1$ and harmonized 230/400 V, three-phase distribution grid, the input current would be 265 A with corresponding connection feeder and fuse. The power, dissipated in the battery, must be withdrawn with proper measures.

IV. GRID CONNECTION DOWNSIZING BY BUFFERING

If the ultrafast charging option is used occasionally – e.g. one EV in two hours or even less, then the EV can be partially decoupled from the grid by using energy buffers [11]…[13]. A decoupling concept is shown in Fig. 3, with main power electronics assemblies:

1. Low power charger (LPC) keeps the SoC to guarantee EV charging power availability and limits the grid load to an average value. It must transmit only charging power for the stationary buffer.
2. High power charger (HPC) charges the EV, drawing energy both from the grid and the buffer. It must transmit the full time-defined charging power.
3. The buffer, based on an electrochemical battery, is connected directly to the dc bus between the LPC and HPC, meaning variable voltage u_{buf} depending on the buffer's SoC.

The buffer output power is defined by the maximal power at the EV charging terminals, available grid power P_g and conversion efficiencies η_{LPC} and η_{HPC}:

$$P_{buf} = \frac{u_{EV} \cdot i_{ch}}{\eta_{HPC}} - \eta_{LPC} \cdot P_g \qquad (8)$$

The effective energy content of the buffer depends on the EV battery capacity and its usable SoC range, losses, available grid power and conversion efficiencies as well as the charging time:

$$E_{buf} = \frac{E_{EV} \cdot \Delta SoC_{EV} + P_{loss,EV} \cdot t_{ch}}{\eta_{HPC}} - \eta_{LPC} \cdot P_g \cdot t_{ch} \qquad (9)$$

In (8) and (9) the pre-fixed variable is P_g. However, the overall energy balance must be kept in mind, so that the buffer could have enough time to recharge before the arrival of the next vehicle. In the next section, the buffering concept will be explained on a demonstrator.

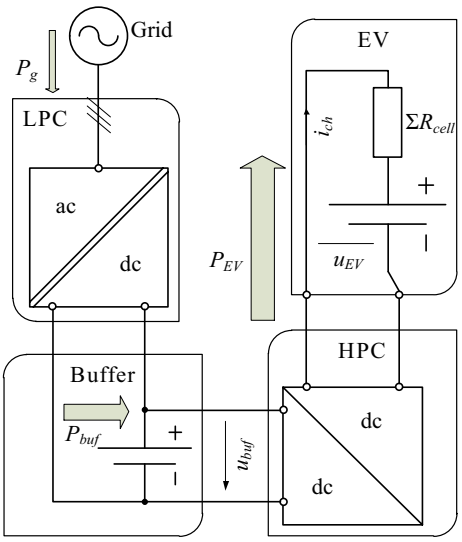

Fig. 3. A buffered EV charging station concept

V. ULTRAFAST CHARGING DEMONSTRATOR

A. Power and energy requirements

The planned demonstrator, fed from a standard industrial three-phase 400 V, 32 A outlet, should be able to recharge an iMiEV or its homologues with data given in Table III within the objective 5 minutes. At given voltage and current ratings with $\cos\varphi \approx 1$, the available grid power equals $P_g = 22$ kW. The conversion efficiencies are estimated rather conservatively $\eta_{LPC} = \eta_{HPC} = 95$ % and the results are shown in Table IV, where EV input power is based on the maximum charging terminal voltage.

TABLE IV. DATA FOR IMIEV BUFFERING

Parameter	Value
$P_g = P_{LPC}$	22 kW
$\eta_{LPC} = \eta_{HPC}$	95 %
P_{buf}	161 kW
E_{buf}	13.5 kW·h
$P_{EV} = P_{HPC}$	173 kW

B. Demonstrator hardware

The LPC is based on a two-stage ac/dc and dc/dc conversion architecture with isolating transformer. It acts as a controlled current source charging the buffer and as limited power source during EV charging following the buffer voltage with increasing current. For smart grid compliance it can be designed bidirectional, supporting energy exchange in both directions.

The HPC topology depends on the differences between u_{buf} and u_{EV}. As u_{buf} varies according to buffer's SoC, the HPC must operate at wide input voltage window. To limit its topology to buck type, the buffer voltage at its minimal SoC must be greater or equal to the EV charging termination voltage:

$$u_{buf,\min} \geq u_{EV}(SoC_{EV,\max}) \qquad (10)$$

The $u_{EV}(SoC_{EV,max})$ value, defined by the number of serial cells and their maximal terminal voltage (Table III), is 361 V, thus the minimal buffer voltage for the next

calculations can be taken $u_{buf,min}$ = 400 V.

For the reasons of mass and volume, the prospective buffer is based on lithium iron phosphate ($LiFePO_4$) cells. The relative continuous discharging current of this electrochemistry is restricted to $i^*_{dch,max}$ = 3 h^{-1}, which accordingly limits the available SoC window [14] [15]:

$$\Delta SoC_{buf} = i^*_{dch,\max} \cdot \frac{t_{ch}}{60} \tag{11}$$

With given values, ΔSoC_{buf} = 25 %, meaning that only a quarter of the buffer's capacity is used effectively. The SoC of the buffer battery should preferably be kept in the region, where charging and discharging voltage alter linearly in time, like between 50 % … 75 %, as shown in Fig. 1 and usual for most lithium-based cells. The number of serial cells in buffer battery

$$n_{buf,s} = \text{round}\left(\frac{u_{buf,\min}}{u_{cell,\min}}\right) \tag{12}$$

The coulomb capacity of the buffer can be calculated from the delivered energy, the available SoC window and the average discharging voltage at given rate:

$$Q_{buf} = \frac{E_{buf}}{u_{buf,dch} \cdot \Delta SoC_{buf}} \tag{13}$$

C. Utilization frequency and efficiency

The buffer has two operating modes: buffering from the grid and charging the EV with the the help of the grid. At constant current buffering, the current is set by the available grid power and terminal voltage.

$$i_{ch} = \frac{P_g \cdot \eta_{LPC}}{u_{buf,ch}} \tag{14}$$

The buffering time is defined by the battery coulomb capacity, usable SoC window and charging current:

$$t_{buf} = \frac{Q_{buf} \cdot \Delta SoC_{buf}}{i_{buf,ch}} \tag{15}$$

The shortest possible charging interval is a sum of buffering and charging times is illustrated by Fig. 4, where negative power values stand for buffering and positive ones for EV charging:

$$t_{int} = t_{buf} + t_{ch} \tag{16}$$

The total efficiency of a buffered charging station can be expressed as the ratio between the useful TTW energy, made available for traction, and the energy, drawn from the grid during interval t_{int}.

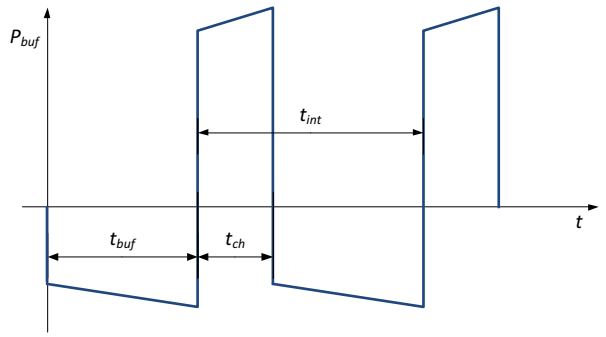

Fig. 4. Charging intervals at buffering and limited grid power

$$\eta_{tot} = \frac{E_{EV} \cdot \Delta SoC_{EV}}{\frac{1}{\eta_{LPC}} \cdot u_{buf,ch} \cdot i_{buf} \cdot t_{buf} + P_g \cdot t_{ch}} \tag{17}$$

D. Numerical results

The cell voltage values at defined SoC and currents were extracted and averaged from datasheets [15], [16]. While relative buffer current values i^*_{buf} were applied, these voltages are supposed to be nearly equal for all $LiFePO_4$ cells independent of the absolute coulomb capacity. The obtained numerical values of (11) ... (17) are shown in Table V.

TABLE V. DESIGN DATA FOR A $LiFePO_4$ BUFFER

Parameter	Value
$i^*_{buf,dch}$	3 h^{-1}
$SoC_{buf,min}$	50 %
$SoC_{buf,max}$	75 %
$u_{cell,min}$	2.90 V
$u_{cell,dch}$	2.92 V
$u_{cell,ch}$	3.35 V
$u_{cell,max}$	3.38 V
$n_{buf,s}$	138
$u_{buf,min}$	400 V
$u_{buf,dch}$	404 V
$u_{buf,ch}$	462 V
$u_{buf,max}$	466 V
Q_{buf}	134 A·h
$i_{buf,ch}$	45.2 A
t_{buf}	44 min
t_{int}	49 min
η_{tot}	72.3 %

At given grid connection the buffered charging station can provide ultrafast charge for an iMiEV in the range of 80 % of its rated battery capacity in less than an hour, or more generally speaking, provide traction energy for a comparable vehicle for the next 85 km (Table II).

The mediocre total efficiency is mainly due to the losses in the buffer and EV battery. The battery roundtrip efficiencies can be improved by overdimensioning, i.e. narrowing the useful ΔSoC, which brings disadvantages in terms of installation space and costs. During each buffering – EV charging cycle, the buffer is being discharged and recharged in SoC window, so its calendric lifetime can be determined if the utilization is known. The cells can be selected from the manufacturer's nomenclature, re-iterating the initially presumed values and eventually using parallel connections for achieving required capacity.

VI. BATTERY FOR THE DEMONSTRATOR

A. General features of lithium iron phosphate cell

The chosen lithium iron phosphate ($LiFePO_4$) cathode chemistry ensures high power density and long battery lifetime. Moreover, it is safe in case of a mechanical damage or electrical abuses such as short circuit, overcharge or depletion. In contradiction to some other cell chemistries, those failures do not cause thermal runaway inside a cell what leads in most cases to an uncontrolled temperature rise and fire.

B. Battery performance using Lishen 130 A·h, $LiFePO_4$ cells

In order to improve parameters given in Table V, the number of cells in battery can be increased; thus, current and losses per cell will be reduced at the cost of the battery weight, explained below. The improved efficiency will shorten required buffering time due to better grid power utilization.

For easier cell performance analysis and testing purposes, the buffering time was fixed to 55 min, so the testing profiles could be the same for cells with different internal resistances and also for the same cell at different currents. As the result, different values for charging power, *SoC* in use and efficiency were obtained for different cell currents.

A simple calculation of buffer efficiency in function of the cell current was made in order to illustrate a relation between the battery mass and efficiency. For calculations the cell was simplified to a series model composed of a voltage source and an internal resistance. The internal resistance was assumed constant in function of *SoC* and any temperature influences were not taken into account.

The input values for calculation are presented in Table IV and Table VI. Additionally, charging time t_{ch} and t_{dis} were assumed as 55 min and 5 min, respectively. The charging current per cell was calculated in order to keep the same flow of electric charge during round-trip cycle according to equation below:

$$i_{ch} = \frac{i_{dch} \cdot t_{dch}}{t_{ch}} \tag{18}$$

The perspective stationary battery is composed of one string of serial cells. Due to difference between charging and discharging currents, the losses of those processes were separately calculated as follows:

$$E_{ch\_losses} = R_{cell} \cdot i_{ch}^{\,2} \cdot t_{ch} \tag{19}$$

$$E_{dch\_losses} = R_{cell} \cdot i_{dch}^{\,2} \cdot t_{dch} \tag{20}$$

In order to calculate efficiency, firstly the internal energy accumulated in the cell was estimated based on the nominal parameters and losses during discharge at nominal current; ΔSoC was calculated according to (11):

$$E_{cont} = (u_{rated} \cdot Q_{nom} + R_{cell} \cdot i_{rated}^{\,2}) \cdot \Delta SoC \tag{20}$$

Knowing the internal energy content of the cell, the total cell efficiency, which is in fact also the buffer efficiency, is calculated as follows:

$$\eta_{buf} = \frac{E_{cont} - E_{dch\_losses}}{E_{cont} + E_{ch\_losses}} \tag{21}$$

The discharge power per cell:

$$P_{dch\_cell} = \frac{E_{cont} - E_{dch\_losses}}{t_{dch}} \tag{22}$$

The approximate battery mass:

$$m_{bat} = \frac{P_{buf}}{P_{dch\_cell}} \cdot m_{cell} \tag{23}$$

Result of calculation for different discharging currents is presented on graph in Fig. 5. For the same profile experimental results were marked by single points on the same graph with data from that test are summarized in Table VII. It should be kept in mind, that at number of serial cells lower than in Table V, HPC in Fig. 3 should be able to boost the input voltage.

The cell was tested at higher current values than the maximum for continuous discharge because of relatively short time of discharge pulse. The test results in Fig. 6 show that temperature increase was not significant and far from upper temperature limit of tested cell. The reason for the smaller temperature increase than anticipated is the low internal resistance in the range 20 % ... 80 % SoC, shown in Fig. 7. The calculation of dc resistance was based on other test results.

TABLE VI. DATA FOR 130 A·H LISHEN CELL

Parameter	Value
Q_{nom}	130Ah
i^*_{max}	2 h^{-1}
u_{rated}	3.2 V
i_{rated}	130A
R_{cell}	1 mΩ
m_{cell}	3.9 kg

TABLE VII. TEST RESULTS OF CELL OPERATION PROFILE

i^*_{dis}	3 h^{-1}	4 h^{-1}	5 h^{-1}	6 h^{-1}
$P^*_{dis\_cell}$	1 132 W	1 462 W	1 776 W	2 090 W
η_{bat}	87.2 %	84.2 %	81.6 %	79.3 %
ΔT	4.0 °C	5.8 °C	8.6 °C	12.7 °C
$n_{cell,s}$	141	110	90	78
m_{bat}	592 kg	429 kg	351 kg	304 kg

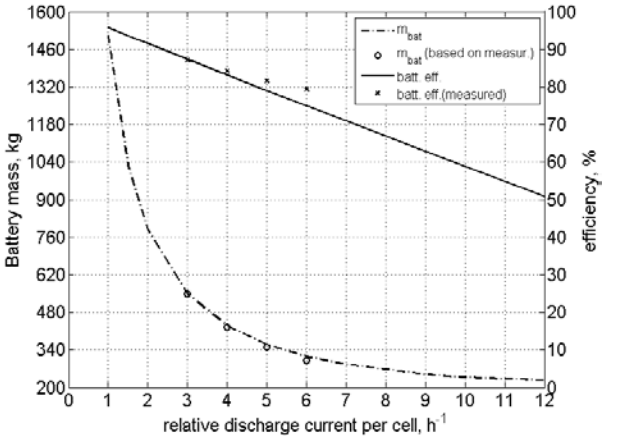

Fig. 5. Battery mass and efficiency in function of cell current

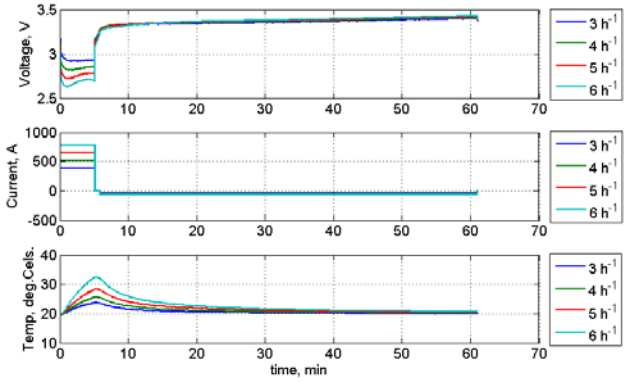

Fig. 6. Test results of cell operation profile for 130 A·h cell at 20 °C

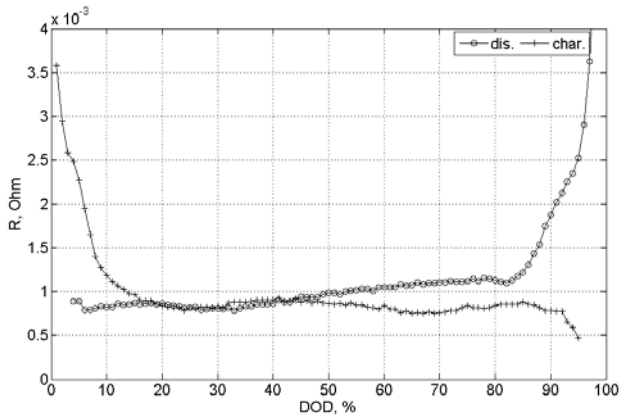

Fig. 7. Internal dc resistance at 20 °C

C. *Discussion on results*

A comparison of efficiency calculation and experimental results in Fig. 5 shows that the calculated efficiency is lower than experimental one. The reason of this fact is temperature influence on the cell resistance which was not taken in consideration. In Fig. 6 it is visible that temperature increases significantly at the end of discharge, therefore the ionic conductivity of electrolyte is increased and efficiency has higher value. Also the temperature change of resistance can be noticed by an increase of cell voltage. A dynamic cell model is already in development, which should take into account transient states of the cell voltage. The model will be used to simulate cell behavior regarding optimal utilization of grid power and take into account variations in power requirement during EV charging, which were more difficult to check in experimentally at the moment.

VII. Conclusion

Throughout this paper, ultrafast charging issues of an EV were studied and a step-by-step design methodology for a buffered ultrafast EV charging proposed. The research yielded following main results:

1. With ultrafast charging, the EV average speed in long distance driving is improved thanks to less time spent at charging stops.
2. The load, imposed to the grid by ultrafast charging, can be leveled by decoupling the vehicle from the mains by the application of energy buffers.
3. With buffering, the EV can be charged from a 400 V, 32 A low voltage outlet, allowing a charging interval of one EV in less than an hour.
4. If more autonomy should be provided in given time and grid power restrictions, buffer capacity and HPC rating must be increased, which means longer buffering times and charging intervals.
5. The partial use of buffer capacity gives a possibility to exploit the battery more effectively at smaller charging and discharging rates, e.g. for grid support (buffer-to-grid applications). However in this variant, the converters and battery must be designed to operate in wider voltage range.
6. With cost, mass and volume restrictions, the buffer is optimally based on lithium iron phosphate cells. Electrochemical storage, however, is related to additional losses thanks to poorer roundtrip efficiency than i.e. ultracapacitors.

The proposed design procedure will be soon implemented on a working demonstrator.

References

[1] Jih-Sheng Lai; D.J. Nelson: "Energy Management Power Converters in Hybrid Electric and Fuel Cell Vehicles," *Proceedings of the IEEE*, vol. 95, no. 4, April 2007, pp. 766-777.

[2] D. Zumkeller: “The German Mobility Panel”. Available online: http://www.mobilitaetspanel.de/

[3] H. Hõimoja, M. Vasiladiotis, A. Rufer: “Power Interfaces and Storage Selection for an Ultrafast EV Charging Station”, *2012 Power Electronics, Machines and Drives Conference*, 27–29 March 2012, 6 p.

[4] IEC 61851-23 Ed 1.0: Electric vehicle conductive charging system - Part 23: d.c. electric vehicle charging station.

[5] T. Anegawa: “Development of Quick Charging System for Electric Vehicle”, *World Energy Congress 2010*, 11 p.

[6] H.M. Magraner: “Ultra-Fast DC Charging Stations”, *ECPE Workshop on Power Electronics for Electric Vehicles*, March 2011, 23 p.

[7] M. Etezadi-Amoli, K. Choma, J. Stefani. “Rapid-Charge Electric-Vehicle Stations”, *IEEE Transactions on Power Delivery*, vol. 25, no. 3, July 2010, pp. 1883-1887.

[8] M. Kamachi, H. Miyamoto and Y. Sano: “Development of power management system for electric vehicle “i-MiEV””, *2010 International Power Electronics Conference*, 21-24 June 2010, pp. 2949-2955.

[9] D. Aggeler, F. Canales et al: "Ultra-fast DC-charge infrastructures for EV-mobility and future smart grids", *2010 Innovative Smart Grid Technologies Conference Europe*, 11-13 Oct. 2010, pp.1-8.

[10] S. Kitano, K. Nishiyama, J. Toriyama, T. Sonoda: “Development of Large-sized Lithium-ion Cell “LEV50” and Its Battery Module “LEV50-4” for Electric Vehicle”, Yuasa Corporation, 2008, 6. p.

[11] S. Bai, Y. Du and S. Lukic, “Optimum design of an EV/PHEV charging station with DC bus and storage system”, *2010 IEEE Energy Conversion Conference and Exposition*, 2010, pp. 1178-1184

[12] G. Joos, M. de Freige and M. Dubois, “Design and Simulation of a Fast Charging Station for PHEV/EV Batteries”, *2010 IEEE Electrical Power & Energy Conference*, 2010, 5 p.

[13] Xie Wei-dong; Luan Wei: "Modeling and simulation of public EV charging station with power storage system," *2011 International Conference on Electric Information and Control Engineering*, 15-17 April 2011, pp. 2346-2350.

[14] H. Huang, T. Faulkner, J. Barker, M.Y. Saidi: “Lithium metal phosphates, power and automotive applications”, *Journal of Power Sources*, vol. 189, April 2009, pp. 748-751.

[15] European Batteries Oy: EV 45 Ah Cell datasheet. Available online: http://www.europeanbatteries.com/

[16] A123 Systems, Inc.: AMP20 Prismatic Pouch Cell datasheet. Available online: http://www.a123systems.com/